



Luminescence Sensitivity of Quartz From Rocks Under *in situ* Chemical Weathering Conditions

Zheng Cao¹, Yingying Jiang², Jiandong Xu^{3,4*}, Juxing Zhao⁵ and Cheng Zhao¹

¹Key Laboratory for Earth Surface Processes, Department of Geography, Peking University, Beijing, China, ²Qinghai Institute of Salt Lakes, Chinese Academy of Sciences, Xining, China, ³State Key Laboratory of Plateau Ecology and Agriculture, Qinghai University, Xining, China, ⁴School of Earth Science and Resources, China University of Geosciences, Beijing, China, ⁵Fujian Exploration Institute of Coalfield Geology, Fujian, China

In provenance investigation of Quaternary sediments, quartz luminescence sensitivity (QLS) has been employed as a technique. The weathering and influence on the earliest signs of luminescence sensitivity of sedimentary quartz require more consideration. In this study, the QLS properties of eight samples of Permian biotite monzogranite from a borehole in the southern tropics of China are investigated. The degree of chemical weathering does not correspond with the QLS values of samples that have undergone varying degrees of *in situ* weathering. We hypothesize that the variation of the irradiation field during the *in situ* chemical weathering process may affect the QLS, but not considerably within 200 ka. In addition, we discovered that quartz from the same source undergoes varying degrees of *in situ* chemical weathering, but has a constant response to irradiation-bleaching cycles (IBCs). The presence of variances in the thermal activation curves (TACs) of the same rock body indicates that further research is required to apply TAC as a provenance indicator.

Keywords: luminescence sensitivity, provenance analysis, weathering index, granite weathering, quartz

OPEN ACCESS

Edited by:

Yuxin Fan,
Lanzhou University, China

Reviewed by:

Shugang Kang,
Institute of Earth Environment (CAS),
China
Ali Abedini,
Urmia University, Iran

*Correspondence:

Jiandong Xu
2018990059@qhu.edu.cn

Specialty section:

This article was submitted to
Quaternary Science, Geomorphology
and Paleoenvironment,
a section of the journal
Frontiers in Earth Science

Received: 10 May 2022

Accepted: 17 June 2022

Published: 15 July 2022

Citation:

Cao Z, Jiang Y, Xu J, Zhao J and
Zhao C (2022) Luminescence
Sensitivity of Quartz From Rocks Under
in situ Chemical
Weathering Conditions.
Front. Earth Sci. 10:940212.
doi: 10.3389/feart.2022.940212

1 INTRODUCTION

Thermoluminescence (TL) and optically stimulated luminescence (OSL) refers to light emission of semiconductors or insulating materials which could store energy in the crystal lattice and emit light under thermally or optically stimulated. TL and OSL have become powerful research tools in the fields of materials (Pires et al., 2011; Kalita et al., 2019; Ike et al., 2021), geosciences (Singhvi et al., 1982; Lai, 2006; Fuchs and Owen, 2008), and environmental and medical science (Higashimura et al., 1963; Yukihiro and McKeever, 2008) in the past two decades. A wide range of natural and artificial materials have been used in the testing of TL and OSL. Quartz is the most prevalent mineral on the earth's surface and has good resistance to weathering and so it is widely used in dosimetry and Quaternary geochronology. However, it was found that the luminescence sensitivity of quartz changed obviously during the dating protocol, which caused an inconsistent response of quartz to radiation dose. Although the change in luminescence sensitivity could be calibrated by a series of well-designed dating protocols, the single aliquot regenerative dose protocols (Murray and Wintle, 2000; Murray and Wintle, 2003), the mechanism is still unclear.

Many studies aiming to calibrate this phenomenon in the laboratory have demonstrated that variations in quartz luminescence sensitivity (QLS) are related to irradiation (Zimmerman, 1971; Benny et al., 2000), bleaching (Li and Wintle, 1992; Zhou and Wintle, 1994) and heating (Rendell

et al., 1994; Bøtter-Jensen et al., 1995; Armitage et al., 2000). Extensive research shows the behaviors of quartz under laboratory conditions, but the reasons for these behaviors are still not clear. Meanwhile, studies focused on the effects of sedimentary transport processes and the characterization of source materials on the QLS have been developed. Aiming to discover and understand the relationships between QLS and the petrological background of quartz, studies have been undertaken in the following areas: the age of intrusive granite (Rink, 1994), crystallization temperature (Sawakuchi et al., 2011b), inclusions (Chauhan and Singhvi, 2019), thermal and sedimentary history (Preusser et al., 2006; Pietsch et al., 2008; Zheng et al., 2009; Fitzsimmons, 2011; Sawakuchi et al., 2011a; Lü and Sun, 2017; Sawakuchi et al., 2018; Chang and Zhou, 2019; Nian et al., 2019; Li and Zhou, 2020; Sawakuchi et al., 2020; Bartyik et al., 2021; del Río et al., 2021). These exploratory efforts have enhanced our understanding of QLS and expanded its application scenarios.

Many new discoveries have also emerged while exploring the QLS of diverse types of sediments, such as aeolian, fluvial and coastal sediments. Different deserts of northern China exhibit discrepancies in QLS and a decreasing trend from east to west, with one exception of the Gurbantunggut Desert (Li et al., 2007; Zheng et al., 2009; Lü and Sun, 2017). Vertical variations in QLS measured from loess-paleosol sequences show a good correlation with other proxies, such as median grain size and magnetic susceptibility, which may reflect climate change or sediment transport dynamic changes (Lü et al., 2014; Qiu and Zhou, 2015; Li and Zhou, 2020; Lü et al., 2020). With an increasing distance of fluvial sediment transportation, sensitizing QLS is observed by Pietsch et al. (2008) and Sawakuchi et al. (2011a), but this growing trend does not always persist. Sawakuchi et al. (2018) considered the QLS as a proxy for denudation rates in the Amazon basin rather than a proxy for transportation distance. In addition, studies using the thermal activation curve (TAC) of quartz to distinguish sediment sources have shown that it appears to be feasible (Chang and Zhou, 2019; Nian et al., 2019; Li and Zhou, 2020).

The variation and characterization of QLS in geological processes from protoliths to sediments requires a deeper and more detailed understanding before it can be applied to a broader range of scenarios. As an important part of the source-sink process, the influence of weathering or denudation on the QLS is still unclear. Previous research (Preusser et al., 2006; Pietsch et al., 2008; Fitzsimmons, 2011; Sawakuchi et al., 2011a; Sawakuchi et al., 2018; Nian et al., 2019; Bartyik et al., 2021; Nelson et al., 2022) have explored that the QLS signature will be modified during the transport process, which could impair the reliability of the QLS as a provenance proxy. However, their studies did not decouple the effects of weathering or denudation from those of transport processes. In this study, quartz extracted from the drill of southeastern China enduring intense *in situ* chemical weathering was evaluated to characterize quartz luminescence sensitivity. Additionally, the applicability of thermal activation curve (TAC) and irradiation-bleaching cycle (IBC) analysis in provenance tracing is discussed. This research has implications for understanding QLS changes caused by *in situ* chemical weathering, as well as evidence for determining whether QLS sensitizing process is dominant under natural conditions.

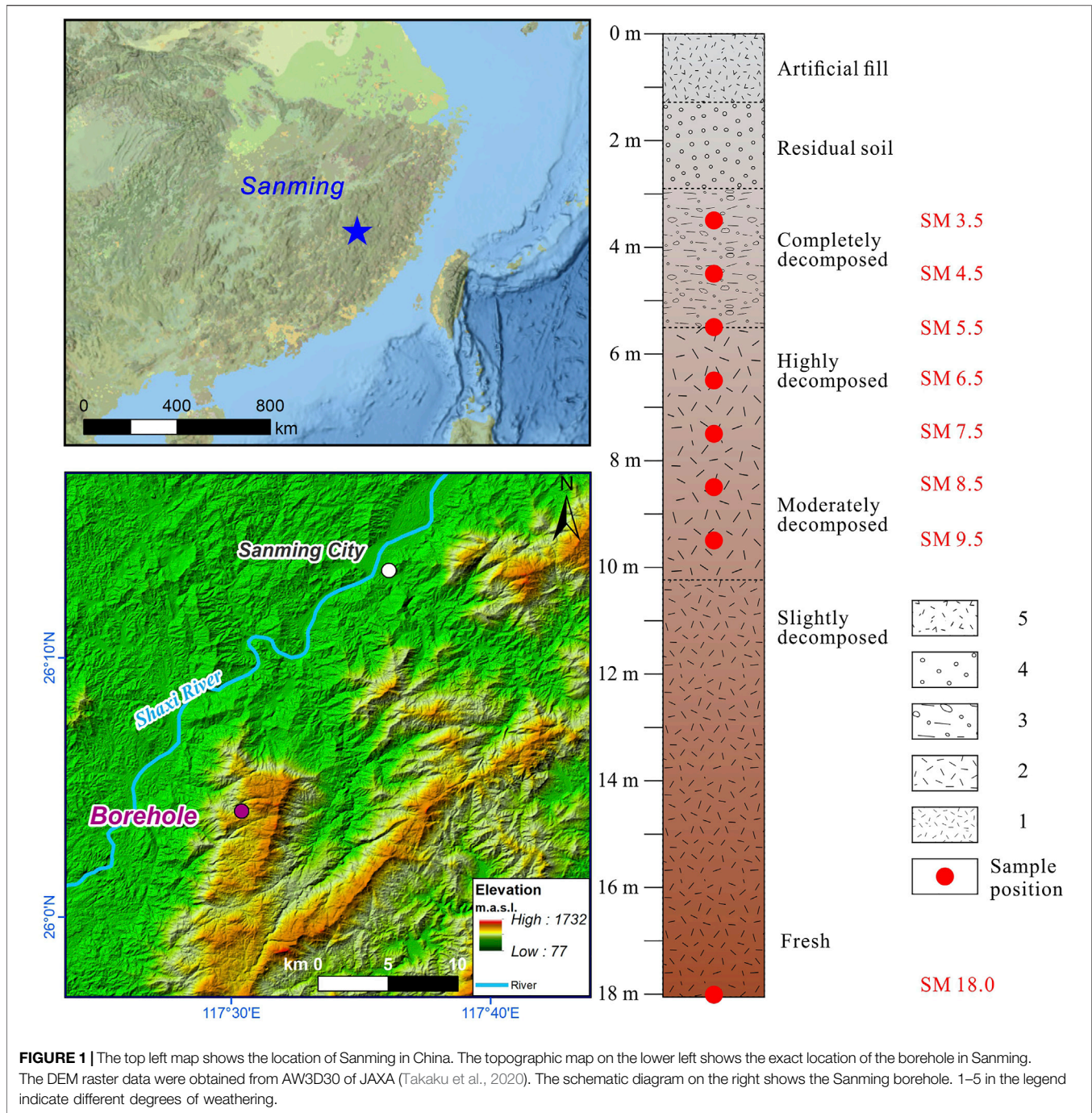
2 GEOLOGICAL SETTING AND SAMPLE

2.1 Geological Setting

The borehole representing chemical weathering conditions is located in the southern part of Sanming city, the subtropical monsoon area of southeastern China, Fujian Province (117.448E, 26.006N). Since the study area is located at the convergence of trade winds and westerlies, the climate is controlled by the couplings of monsoon and subtropical highs. In general, the summer (May–September) climate character of the study area is hot and rainy, while it is warm and relatively dry in winter (December–January). The climate data for the study site are for the period 1981–2010 and are from the China Meteorological Data Service Centre (data.cma.cn). The annual average temperature in the Sanming area is 19.6°C, with extreme high temperatures reaching 41.4°C. The average number of days with maximum temperatures above 30°C over the years is 122.8. Precipitation is plentiful throughout the year, with an average annual precipitation of 1,665.2 mm and a maximum continuous precipitation (day) of 444 mm (15 days) over the years. In addition, the study area was also affected by typhoons in summer. All the above conditions resulted in a relative humidity reaching 78% in study area over the year. In summary, the Sanming area is a typical area of intense chemical weathering.

The study area is located in the western part of the Zhenghe-Dapu fault zone, which belongs to the northern end of the Yongmei sag. After the convergence of the Cathaysia and Yangzi blocks as part of the Rodinia supercontinent in the early Neoproterozoic (Li et al., 2002), the study area gradually broke up into rift valleys or troughs during supercontinent rifting, and formed giant thick marine deposits during the late Neoproterozoic to Early Paleozoic (Shu, 2012; Shu et al., 2021). With the strong tectono-thermal events in South China during the Silurian, the sediments were deformed and uplifted by compression. At the same time, magmatic activity was frequent, forming a large number of S-type granites and fewer I-type granites (Shu, 2006). The super-thick dolomite and limestone from the Early Paleozoic until the Early Triassic reflect a slow south-to-north transgression (Zu et al., 2012). The study area received strong north-south extrusion during the Indo-Chinese period leading to crustal thickening, accompanied by large-scale magmatic activity (Zhang et al., 2009). During the Cretaceous period, the study area was characterized by three-stage tectono-thermal events and andesites and rhyolites caused by strong volcanic activities (Li et al., 2014). During the Cenozoic period, continuous subduction of the Pacific plate resulted in regional uplift and denudation of the study area (Bureau of Geology and Mineral Resources of Fujian Province, 1985).

In the study area the basement is covered by effusive rock strata and sedimentary rocks formed from Paleozoic to Cenozoic. Both strata and intrusive rocks have undergone intensive tectonic movements, resulting in unformed and discontinuous strata. The Quaternary strata are remnants of alluvium and floodplain, consisting of clay, sand, gravel and rock fragments, with uneven thickness distribution. The residual slope deposits are widely distributed in mountains, gullies and gentle hills, while the alluvial deposits are mainly distributed in river valleys. Small flat Quaternary terraces, small basins connected by the Shaxi River, and low hills constitute the main geomorphic type in the study region.



2.2 Sample

The drill was conducted by the Fujian Exploration Institute of Coalfield Geology, penetrated Quaternary sediments and regolith, finished in the body of Permian greyish medium-grained biotite monzogranite, at a depth of 18.1 m. According to the field work, the drill core was divided into 5 layers: I. human activities disturbed layer (0~1.3 m); II. Quaternary sediments or residual soil layer (1.3~2.9 m); III. completely weathered rock (2.9~5.6 m); IV. highly weathered rock (5.6~10.2 m); V. moderately weathered to fresh rock (10.2~18.1 m). To avoid human interference or sediments

from different sources, we sampled 8 weathered rocks from 3.5 to 18.0 m, and the specific positions are shown in the map on the top left of the **Figure 1**.

3 METHODS

3.1 Quartz Sample Preparation

All the granitic rocks were crushed and ground after washing with distilled water. The samples for element analysis were ground into

powder (diameters < 40 μm) without any separation. The samples for luminescence analysis were crushed and ground, and mixed grains between 180 and 250 μm were selected by wet sieving. The grains were treated with 10% HCl and 30% H_2O_2 solutions to remove carbonates and organic matter, and then heavy liquids of 2.62 and 2.75 g/cm^3 were used to separate quartz and plagioclase from heavy minerals and potassium feldspar (Aitken, 1998). As quartz and plagioclase have similar densities, 40 min HF etching was used to remove the latter. Using differences in hydrodynamics, micas were also removed from the system, preventing their luminescence from affecting the weak luminescence of the rock (Kortekaas and Murray, 2005). Quartz grains were checked by using the X-Ray Diffraction (XRD) and OSL IR depletion ratio (Duller, 2003) to qualify the purity after etching. The mass of aliquots of adhered quartz grains was weighed with a Mettler Toledo XPR10 microbalance with a precision of 1 μg . The average mass on each aliquot is approximately 4–6 mg. The details of the sample preparation protocol are described in the **Supplementary Materials**.

3.2 Luminescence Analysis

3.2.1 Equipment

All luminescence measurements were conducted on a Lexsy Smart TL/OSL Reader at Peking University, which was equipped with an IR laser diode ($850 \pm 3 \text{ nm}$, up to $400 \text{ mW}/\text{cm}^2$ at the sample position) and 5 blue LEDs filtered by 3 mm Schott GG455 glass ($458 \pm 10 \text{ nm}$, up to $100 \text{ mW}/\text{cm}^2$ at the sample position). A homogeneous irradiation field is provided by a specially designed circular arranged Beta (^{90}Sr - ^{90}Y , 1.6 GBq) source (Richter et al., 2012). Bi-alkaline photomultiplier tubes (Hamamatsu H7360-02, 300–650 nm) with quantum efficiencies of approximately 27% at 400 nm are used for receiving signals (Richter et al., 2013).

3.2.2 Procedures of Measurements of Quartz Luminescence Sensitivity, Irradiation-Bleaching Cycles, and Thermal Activation Curves

The luminescence sensitivity of quartz was measured following the procedures (Table 1). First, the aliquot was bleached enough long (120–180 s) by blue light at 125°C to reduce the quartz signal to the background level, and 11.25 Gy beta dose was given to the sample after bleaching. Second, the aliquot was heated to 220°C to measure the TL signal responding to the given dose, and the integration from 70 to 120°C of the signal was used to calculate the quartz 110°C TL intensity. Next, infrared stimulation was used to ensure that the signal of feldspar inclusions would not affect the quartz OSL sensitivity. Finally, the quartz OSL was obtained by 115 s blue stimulation at 125°C , and the signal for the initial 2 s minus the background value was summed to represent the OSL intensity. A stimulated temperature of 125°C reduces the probability of retrapping by traps when electrons recombine with holes. According to the definition of luminescence sensitivity, we used mass and given dose to normalize quartz 110°C TL and OSL intensity as sensitivity, respectively. Each sample was represented by five aliquots accurately weighed on a microbalance at the 1 μg level.

The measurements of irradiation-bleaching cycles (IBCs) are the loop of QLS measurements. To reduce the amount of data and test time, only signals at specific loops were recorded.

The protocol for measurements for TAC was the same as that for the QLS and is shown in Table 2. The differences between them are the step of thermal activation before beta dose is given.

3.3 Weathering Analysis

For the purpose of evaluating chemical weathering indices, X-ray fluorescence (XRF) is a rapid and convenient method for whole-rock analysis. A wavelength dispersive (WD) XRF (Rigaku ZSX Primus II) at the State Key Laboratory of Plateau Ecology and Agriculture was used to analyze major elements in the whole-rock powder in the ppm to 100% range. The crushed and ground samples mentioned in Section 3.1 were dried in a vacuum drying chamber for 8 h at 110°C to remove moisture. Loss on ignition (LOI) was determined by heating a 2–3 g sample in a muffle oven at $1,050^\circ\text{C}$ for 1 h and weighing immediately after cooling in a desiccator to avoid absorption of air moisture. Samples (3–4 g) were placed into a plastic ring (diameter of 35 mm) without any binder and pressed into a discoidal pallet under 400 bar for 2 min. XRF results were output as the mass percentage of major elements adjusted by LOI and were converted to the molar proportion to calculate the chemical weathering indices.

The mineralogy of the whole-rock powder was determined by X-ray diffraction (XRD) with a Rigaku D/Max 2500PC equipment with radiation from $\text{CuK}\alpha$ ($\lambda = 1.5406 \text{ \AA}$) at 40 KV and 200 mA. We obtained diffractograms of air-dried mounts for a 2θ range from 3° to 70° at a scanning speed of $8^\circ/\text{min}$. Panalytical Highscore software and crystallographic information file (CIF) from Crystallography Open Database (Vaitkus et al., 2021) were used to identify minerals and calculate mineral proportions by semi-quantitative methods.

4 RESULTS

4.1 Quartz Luminescence Sensitivity Signatures in Sanming Borehole

The quartz luminescence sensitivity variations in the Sanming borehole, monitored by 110°C TL and OSL, did not exhibit an obvious trend with the change in depth, as shown in Figure 2 and Table 5. The distribution of data for 110°C TL sensitivity was relatively concentrated, falling within the range of 141.7–99.6 counts/(Gy*mg). The OSL sensitivity values were small overall with slight fluctuations and distributed in the range of 22.6–27.9 counts/(Gy*mg). Both the QLS of the 110°C TL and OSL showed fluctuating patterns of variation along depth, but the former showed a gradual increase along depth above 6.5 m. A total of 40 aliquots for all 8 samples are projected in an X-Y coordinate system with OSL sensitivity and 110°C TL sensitivity as axes. As in Figure 3A, the data points representing all the 40 aliquots are almost clustered together and do not show clear distinguishability.

Using the R package numOSL (Peng et al., 2013), we analyzed the composition of the luminescence signals of eight samples with different degrees of weathering. CW-OSL is considered to be resolved into three components based on their decay rates (Smith

TABLE 1 | Protocol for measurements of quartz luminescence sensitivity (QLS) and sensitivity response to irradiation-bleaching cycles (IBC).

Step	Procedure	Observe
1	Blue light bleaching 180 s at 125°C, 50 mW/cm ²	110°C TL S _n (n = 0, 1, 2, 5, 10, 15, 25)
2	Beta irradiation, 11.25 Gy	
3	TL (5 K/s from 25 to 220°C, 10 s)	
4	OSL IR Laser for 120 s at 25°C	
5	OSL Blue LED for 115 s at 125°C, 50 mW/cm ²	OSL S _n (n = 0, 1, 2, 5, 10, 15, 25)
6	Go to step 1 for next cycle	

TABLE 2 | Protocol for measurements of thermal activation curves (TAC).

Step	Procedure	Observe
1	Blue light bleaching for 120 s at 25°C, 50 mW/cm ²	110°C TL S _n (n = 0,1,2...)
2	Heat to T °C (Initial T = 200°C) for 60 s, 5K/s	
3	Beta irradiation, ~ 11.2 Gy	
4	TL (5 K/s from 25 to 220°C, 10 s)	
5	OSL Blue LED for 40 s at 125°C, 50 mW/cm ²	OSL S _n (n = 0,1,2...)
6	Go to step 1, T = T + 40°C	

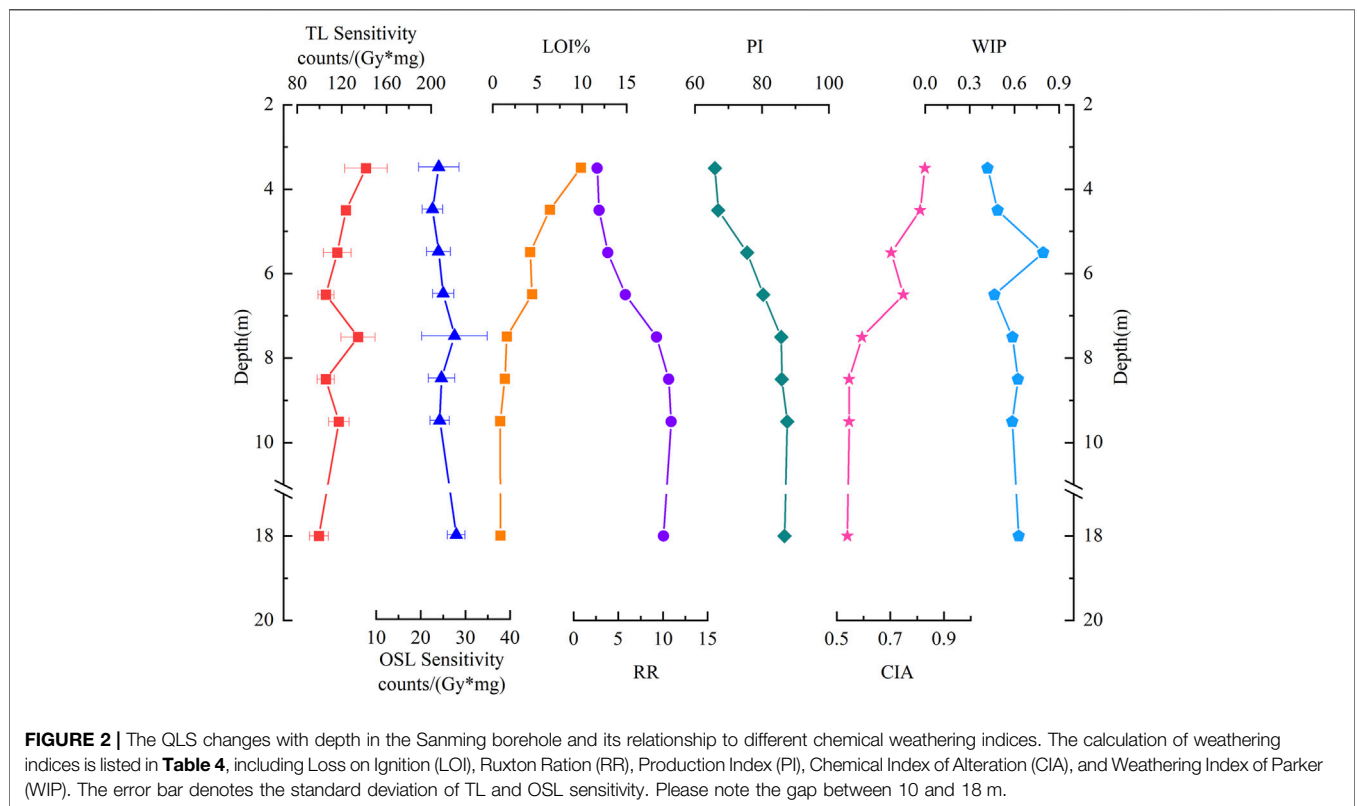


FIGURE 2 | The QLS changes with depth in the Sanming borehole and its relationship to different chemical weathering indices. The calculation of weathering indices is listed in **Table 4**, including Loss on Ignition (LOI), Ruxton Ration (RR), Production Index (PI), Chemical Index of Alteration (CIA), and Weathering Index of Parker (WIP). The error bar denotes the standard deviation of TL and OSL sensitivity. Please note the gap between 10 and 18 m.

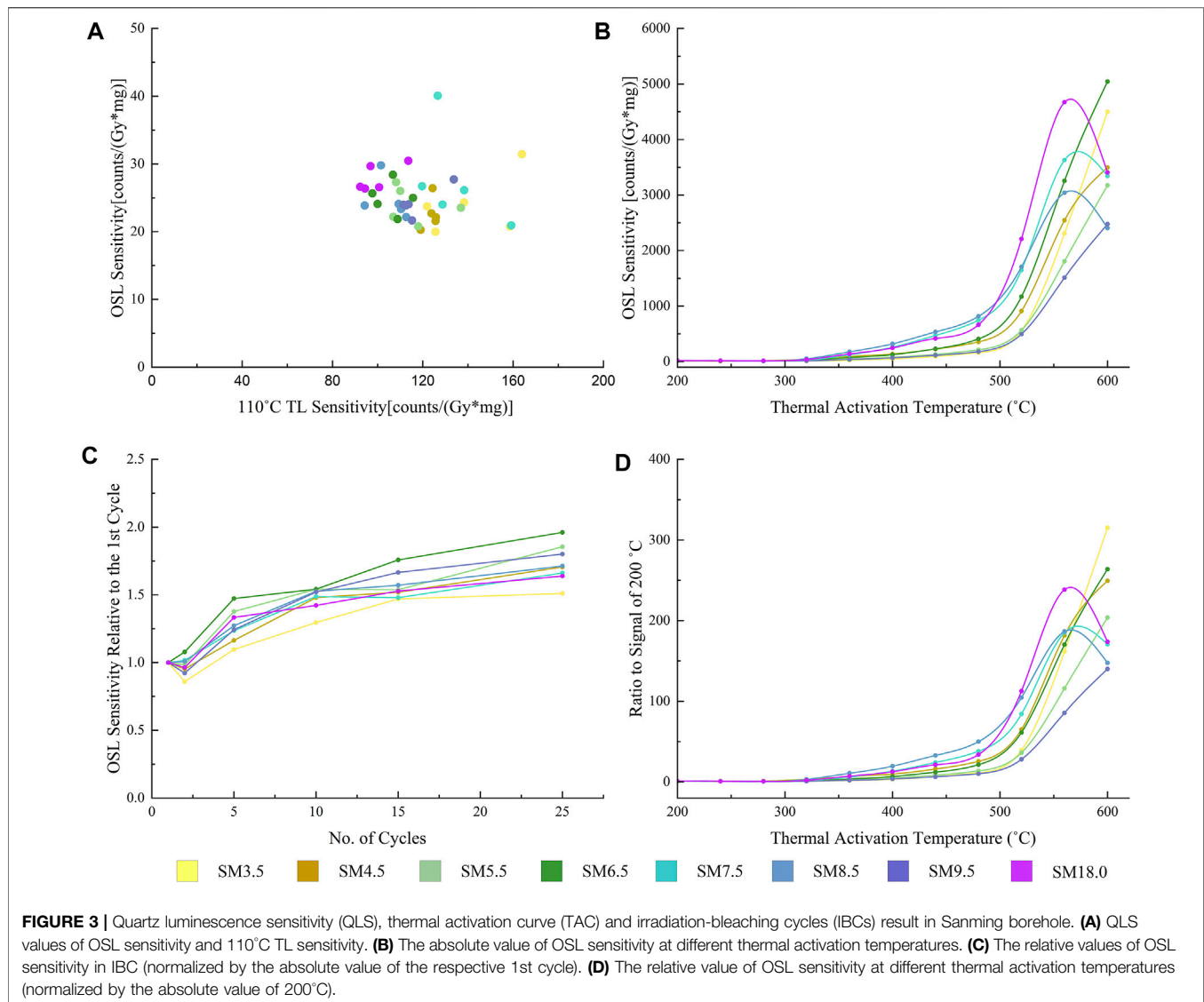
and Rhodes, 1994), which are fast, medium and slow component. The decay curves were fitted according to equation given below:

$$I(t) = I_{00} + I_{01}e^{-\lambda_1 t} + I_{02}e^{-\lambda_2 t} + I_{03}e^{-\lambda_3 t}$$

where $\lambda_1, \lambda_2, \lambda_3$ are the decay rate related to electron detrapping cross-sections, and I_{0k} ($k=1,2,3$) are initial luminescence signal intensity related to the initial populations of electrons in traps

(Bluszcz and Adamiec, 2006; Zhou et al., 2010), and I_{00} is a constant component and is regarded as a background signal.

Figure 4 shows the decay curve raw data and the three components, where the sum of slow component signal and the background signal are shown as a separate item. It can be observed that all samples are dominated by the slow component. After 10 s of stimulation, the samples contain



almost no fast and medium components, and the slow components decay at a steady low rate. **Figure 5** shows the relative proportions of the three components as a function of excitation time. We noticed that the top 4 samples of borehole had more fast components than the bottom samples. The percentage of “BG+Slow Component” signal (sum of slow component and background signal) for the top 4 samples reached 95% at 5.0 s and 90% at 1.5 s on average. In contrast, the bottom 4 samples reached this ratio much faster, at 2.6 and 1 s, respectively.

4.2 Chemical Weathering Parameters in Sanming Borehole

Table 3 shows the weight percentages of the major chemical elements measured by XRF and adjusted by the LOI parameter. From the bottom to the top of the borehole, Na_2O , K_2O , SiO_2 , and CaO decreased upwards, while Al_2O_3 and iron oxides Fe_2O_3

increased significantly with increasing degree of weathering. MgO , P_2O_5 , TiO_2 , and MnO did not exhibit any obvious trends with depth. LOI parameters were calculated and are listed in **Table 3**, which also increases with the observed grade of chemical weathering in field. In general, with the decreasing depth of the borehole, soluble and mobile elements were removed, while immobile and nonsoluble elements increased relatively. Although the trend of the concentration of the above elements in the borehole is obvious, there are still some exceptional points, and the reasons for these points will be discussed in **Section 5.1**.

4.3 Mineralogy Evidence of Weathering

The XRD spectra of 8 samples from the Sanming drill hole at different depths were compared and are shown in **Figure 6**. Overall, there is consistency between the 8 spectra, but there is also variation. It can be clearly seen that the strongest peak ($2\theta = 26.59^\circ$) in all samples at different depths is from the quartz

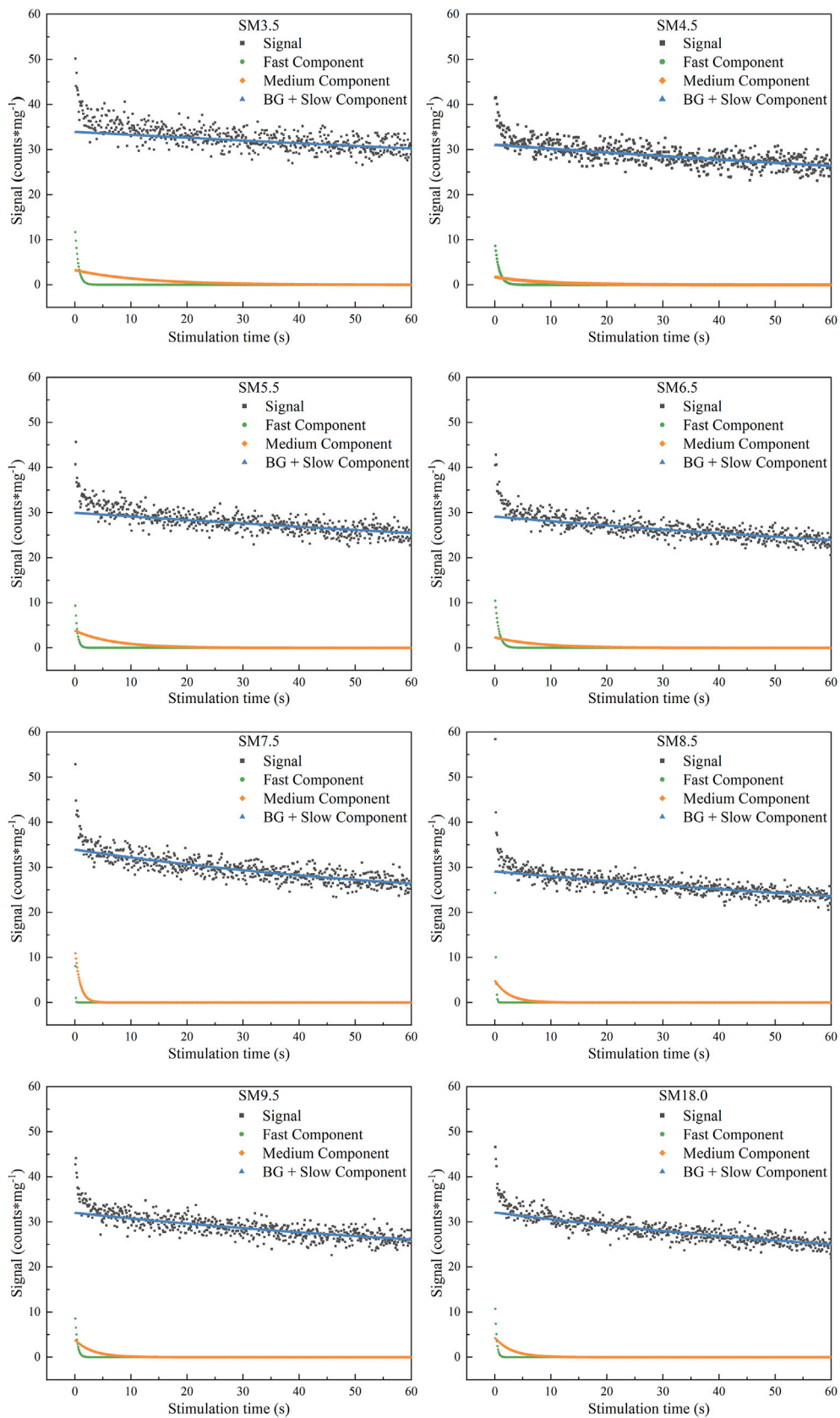


FIGURE 4 | The decay curves of 8 samples and the fast, medium and slow components obtained after curve deconvolution. Since the fast and medium components decayed rapidly to zero and the slow component decayed at a constant rate, only the first 60 s of data were intercepted and plotted.

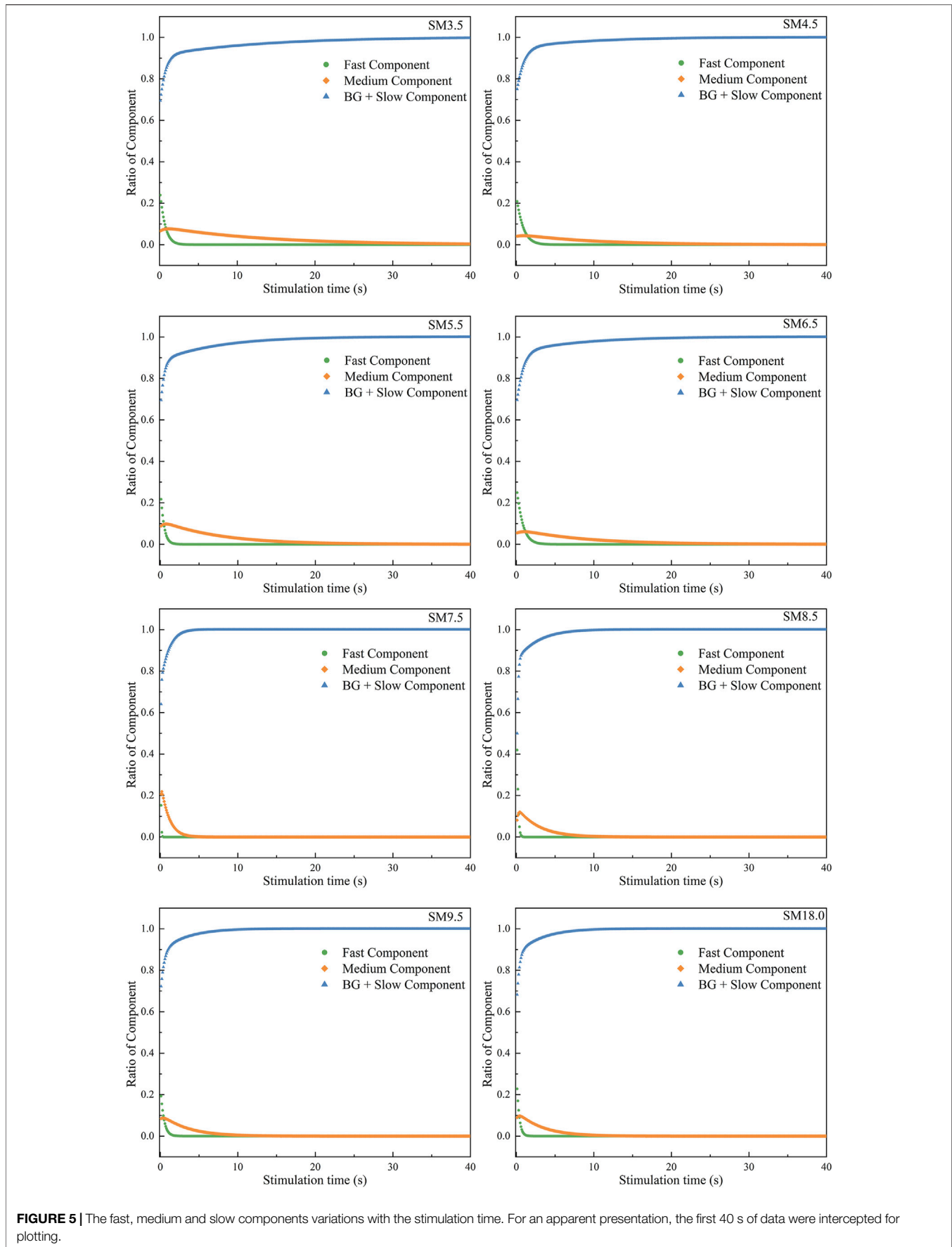


FIGURE 5 | The fast, medium and slow components variations with the stimulation time. For an apparent presentation, the first 40 s of data were intercepted for plotting.

TABLE 3 | Major chemical element weight percentage (%) and LOI of Sanming Borehole.

No.	LOI%	Na ₂ O	MgO	Al ₂ O ₃	SiO ₂	P ₂ O ₅	SO ₃	K ₂ O	CaO*	TiO ₂	MnO	FeO(total)	ZnO	NiO	V ₂ O ₅	BaO	PbO	Cr ₂ O ₃	SUM
SM3.5	9.87	0.0000	0.1028	27.9188	43.1170	0.0315	0.0000	4.8157	0.2999	1.7449	0.0971	11.9372	0.0314	0.0123	0.0178	0.0000	0.0000	0.0000	100.0000
SM4.5	6.42	0.0000	0.0540	26.8693	45.1917	0.0619	0.0000	5.7116	0.0405	1.7484	0.1131	13.6571	0.0000	0.0000	0.0000	0.1338	0.0000	0.0000	100.0000
SM5.5	4.19	0.0351	0.0498	24.0848	54.3018	0.1046	0.0000	9.2729	0.0466	1.1927	0.0932	6.3876	0.0000	0.0000	0.0000	0.2386	0.0000	0.0000	100.0001
SM6.5	4.41	0.0331	0.0702	17.9551	61.4402	0.0887	0.0250	5.4159	0.0553	1.3307	0.1943	8.9616	0.0240	0.0000	0.0000	0.0000	0.0000	0.0000	99.9999
SM7.5	1.58	0.2917	0.0748	12.5538	68.7137	0.1389	0.0000	6.3863	0.6420	1.2630	0.1882	8.0081	0.0177	0.0000	0.0000	0.1138	0.0000	0.0264	100.0001
SM8.5	1.36	0.2066	0.0702	10.8863	68.2633	0.1525	0.0000	6.9077	0.6663	1.3575	0.0000	9.9735	0.0274	0.0000	0.0000	0.1279	0.0000	0.0000	100.0001
SM9.5	0.82	0.2412	0.0693	11.0754	71.3314	0.1054	0.0210	6.2855	1.1055	0.9974	0.2639	7.5587	0.0526	0.0000	0.0000	0.0000	0.0174	0.0447	99.9896
SM18.0	0.87	0.3341	0.0992	11.7575	69.7376	0.1566	0.0000	6.6223	1.2620	0.9682	0.1609	7.9748	0.0000	0.0000	0.0000	0.0000	0.0000	0.0538	100.0000

CaO*: silicate bond and Carbonate bond CaO.

mineral, as it is the most weathering resistant mineral. The plagioclase decreased with increasing weathering and was not even visible in samples above 6.5 m. The peaks of mica also gradually disappeared in the samples above 6.5 m. The characteristic peaks of kaolinite or chlorite ($2\theta = 12.40^\circ$) and illite ($2\theta = 19.85^\circ$) can be clearly seen in the sample at 3.5 m.

4.4 Irradiation-Bleaching Cycles and Thermal Activation Curves in Sanming Borehole

We assessed the IBC values of 8 samples from the Sanming borehole, and each of them were normalized by the respective first cycle value. As shown in Figure 3C, the 8 samples at different depths exhibit relatively the same trend of variation. The normalized IBC values grew gradually with the increase in the number of cycles. After the 1st, 2nd, 5th, 10th, 15th, and 25th cycles, the normalized IBC values of all samples did not show a large dispersion. The normalized IBC values gradually increased from 0.9 to 1.1 at the first cycle to 1.5–2.0 at the last cycle. Additionally, we noticed that some samples (SM5.5) maintained a faster increasing trend after the last cycle, while some samples (SM3.5) remained almost unchanged.

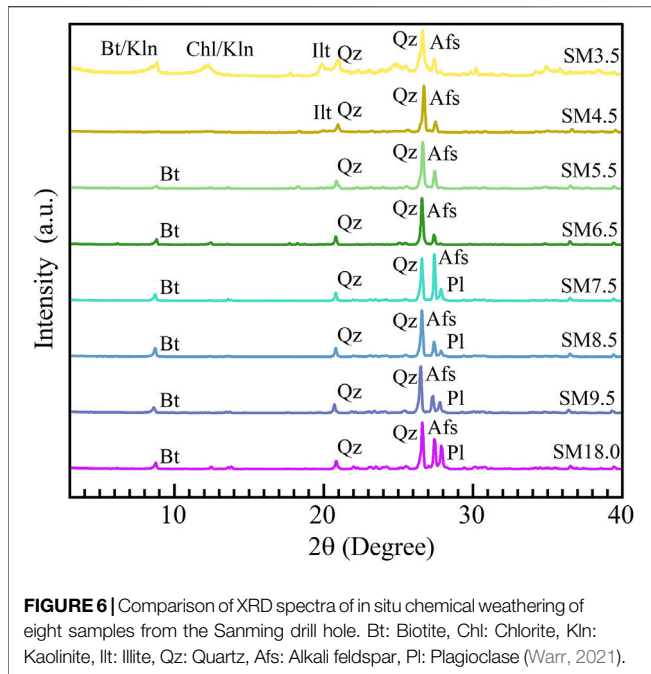
We performed TAC experiments in the interval from 200 to 600°C, with one measurement at each temperature rise of 40°C. The absolute values of the TAC test results are presented in Figure 3B., showing the variations of OSL sensitivity under thermal activation temperatures. The absolute values of TAC of the 8 samples remained almost constant for the measurements before 320°C. As the heating continued, the absolute values of the samples had a faster rise and a larger difference. The 8 samples were divided into two parts: one part reached the peak and subsequently dropped back (SM7.5, 8.5, 18), and the other part continued to increase (the other 5 samples). In Figure 3D., the absolute value of OSL sensitivity is normalized by the respective value of 200°C and the same pattern is also found in the normalized results.

5 DISCUSSION

5.1 Quartz Luminescence Sensitivity Constrained by Chemical Weathering

In a normal chemical weathering process under humid-warm climate conditions, hydrolysis results in silica movement in a profile, that is, irregular and small, while alkali and alkaline earth metals are greatly depleted (Parker, 1970). The common principle of weathering indices assumes that the major element distribution in parent rock is homogeneous on a certain scale, and the initial weathering degree is equal or the weathering starting line is the same for the samples.

Different weathering indices have been introduced to estimate the degree of weathering for various weathering conditions or weathering matrix. Although more than 30 different weathering indices were introduced, 5 indices applicable to granite, including RR (Ruxton Ratio), PI (Product Index), CIA (Chemical Index of Alteration), WIP (Weathering Index of Parker) and LOI, were



chosen to evaluate chemical weathering intensity or extent in quantitative rather than qualitative terms in the current experiment. The Ruxton (1968) has been proven to be a good index for acidic or felsic rocks, and it assumes that alumina and other sesquioxides are immobile during weathering. WIP (Parker, 1970) is based on bond strength with oxygen and the proportion of mobile major elements (i.e., Na, K, Mg and Ca). CIA (Nesbitt and Young, 1982) applies the molecular ratio between immobile and mobile major elements, reflecting the conversion of feldspars to clays. LOI assesses weathering by calculating OH^- ions during the weathering process and ignoring a small amount of other volatiles (Sueoka et al., 1985; Gupta and Rao, 2001). **Tables 4, 5** summarize and express specific calculation formulas and results.

PI and RR decreased as the grade of weathering increased, LOI and CIA increased as the grade of weathering increased, while WIP did not show an expected tendency as shown in **Figure 2**. It demonstrated a gradual decreasing weathering effect from 3.5 to 7.5 m and a nearly constant trend from 7.5 to 18.0 m. The initial results of major elements are compatible with the phenomena observed in the field work. Both WIP and CIA exhibited the same variation trend with an odd point at a depth of 5.5 m, where the potassium content was higher than that at all other points, which caused abnormalities in the indices. In contrast, PI employ a calculation method similar to that of CIA or WIP but does not involve potassium, so it gradually increases with depth until it plateaus without outliers. The LOI increased continuously with increased weathering, representing the value of OH^- in the secondary mineral formation, which is the residual of weathering.

The mineralogical results show that the fresh granite of the Sanming borehole is mainly composed of quartz, plagioclase, alkali feldspar and biotite. With increasing weathering, feldspar and mica chemically decomposed and transformed into hydrous

clay minerals, such as kaolinite, illite and chlorite. Our experiments demonstrate from the mobility of chemical elements and the transformation between minerals that chemical weathering of the borehole is present and gradually increases from the bottom to the top.

QLS could be affected by congenital or acquired factors, such as crystallization (Sawakuchi et al., 2011b), inclusions (Chauhan and Singhvi, 2019), irradiation (Zimmerman, 1971; Benny et al., 2000), bleaching (Li and Wintle, 1992; Zhou and Wintle, 1994), or thermal history of quartz grains. The Sanming borehole, penetrated the weathering layer, was drilled on a Carboniferous granitic pluton that crops out on the surface and occupies an area of approximately 80 km^2 . Compared to the large pluton, the heterogeneity of minerals in the borehole should be ignored, and quartz grains should be considered to have the same crystallization conditions, thermal history, and similar composition. Moreover, *in situ* weathering conditions do not allow quartz to enter the loop of irradiation-bleaching cycles (IBCs), which have already been proven to lead to an increase in QLS (Pietsch et al., 2008). Thus, the most likely factors affecting QLS are 1) the variation intensity of irradiation due to the changes in the radiation field, 2) the absorbed dose after being shielded by water, and 3) the dissolution of the surface layer of quartz by water. During the weathering process, the migration of radioactive elements would change the radiation field significantly (Jeong et al., 2007). For example, the alpha dose rate (Gy/ka) per ppm for the natural uranium series is 2.78, and the beta dose rate is 0.7982 Gy/ka for natural potassium at a 1% concentration (Adamiec and Aitken, 1998; Guérin et al., 2011). The pores and fractures of granite increase with the intensity of weathering, providing space for water to shield quartz grains against α , β , and γ radiation, which results in quartz gains receiving varying radiation doses during the chemical weathering process. Water not only protects the quartz grains from radiation but also dissolves them. Although the dissolution of quartz at 25°C and at neutral pH is slight ($\sim 10^{-14.5}$ to $10^{-15.1} \text{ mol/m}^2/\text{s}$) (Schulz and White, 1999), it is also possible to affect the morphology of quartz by creating etch pits and fragmentations that may have effects on QLS. Meanwhile, the gradual expansion of pores and fractures provides channels for radon to escape, which decreases the subsequent radioactive decay chain and intensity of the radiation field. Overall, the main factors that may affect the QLS in the Sanming borehole are fluctuations in the radiation field in the historical period, which are caused by dissolution of quartz grains, water shielding and migration of radioactive elements.

It is quite difficult to recover the radiation field controlled by such complex conditions in the historical period. The chemical weathering process may be regarded as a black-box model combining three input variables: radiation field, water shield, and dissolution of quartz surface. Sawakuchi et al. (2018) considered that a longer duration of chemical weathering increases the QLS, which accounts for the high-sensitivity quartz in the cratonic areas of the Central Brazil shield. In our results, the relationship between OSL sensitivity and chemical weathering indices was not significant in the *in situ* chemical weathering scenario, indicating that the OSL

TABLE 4 | Chemical weathering indices used in this study.

Weathering Index	Formula	Ideal Tendency with Degree of Weathering	References
CIA (Chemical Index of Alteration)	$\text{Al}_2\text{O}_3/(\text{Al}_2\text{O}_3 + \text{K}_2\text{O} + \text{CaO}^\dagger + \text{Na}_2\text{O}) \times 100$	Increase	Nesbitt (1979), Nesbitt and Young (1982)
PI (Product index)	$\text{SiO}_2/(\text{SiO}_2 + \text{TiO}_2 + \text{Fe}_2\text{O}_3 + \text{FeO} + \text{Al}_2\text{O}_3)$	Decrease	Reiche (1943)
RR (Ruxton ratio)	$\text{SiO}_2/\text{Al}_2\text{O}_3$	Decrease	Ruxton (1968)
WIP (Weathering Index of Parker)	$(\text{CaO}^\dagger/0.7 + 2\text{Na}_2\text{O}/0.35 + 2\text{K}_2\text{O}/0.25 + \text{MgO}/0.9) \times 100$	Decrease	Parker (1970)
Loss on Ignition	H_2O (+and-)	Increase	Sueoka et al. (1985)

CaO[†]: silicate bond CaO.

TABLE 5 | Quartz luminescence sensitivity and chemical weathering indices for samples from Sanming Borehole.

Depth (m)	OSL	Standard deviation	TL	Standard deviation	CIA	PI	RR	WIP	LOI %
	Sensitivity		Sensitivity						
	counts/(Gy*mg)		counts/(Gy*mg)						
3.5	24.045	4.534	141.677	18.987	0.829	65.957	2.621	0.419	9.874
4.5	22.618	2.309	123.745	2.750	0.811	66.973	2.854	0.488	6.419
5.5	23.965	2.680	116.015	12.436	0.703	75.635	3.826	0.793	4.192
6.5	25.001	2.386	105.790	7.199	0.749	80.427	5.807	0.466	4.406
7.5	27.573	7.351	134.527	15.309	0.595	85.813	9.289	0.588	1.582
8.5	24.649	2.972	105.629	7.605	0.547	85.918	10.642	0.625	1.361
9.5	24.257	2.176	117.331	9.272	0.546	87.575	10.930	0.586	0.820
18.0	27.940	1.972	99.569	8.431	0.540	86.744	10.066	0.628	0.873

sensitivity was less sensitive to three variables together. TL sensitivity monitored by 110°C exhibits a trend consistent with the intensity of chemical weathering. As the borehole is only 18 m in depth, and we cannot speculate whether the QLS would have remained constant if weathering had proceeded. However, we can conclude that 110°C TL sensitivity is more responsive to chemical weathering under the same conditions. This can also be noticed in previous work (Lü et al., 2014; Lü and Sun, 2017; Li and Zhou, 2020; Lü et al., 2020), where quartz in Paleosol or Pedocomplex has a higher QLS compared to loess, and the luminescence sensitivity of TL is several times higher than that of OSL. The difference, however, is that our QLS values are in the tens to hundreds of percent of the values in the above literature. Yang and Zhou (2019) used the uranium disequilibrium method to estimate that the chemical weathering rate of granite is 0.038 mm/year in the northern part of Guangdong Province, a mountain area with weathering conditions close to Sanming. We assume that samples above 7.5 m were weathered at the rate described above and concluded that the QLS caused by the variate intensity of irradiation will not change significantly in at least 200 ka under such weathering conditions.

5.2 Irradiation-Bleaching Cycles and Thermal Activation Curves

Changes in the luminescence sensitivity of quartz particles during irradiation-bleaching cycles (IBCs) have been extensively studied. Some of the studies have yielded a good linear correlation between the increase in QLS and the increase in the number of IBCs (Preusser et al., 2006;

Pietsch et al., 2008; Zheng et al., 2009; Chang and Zhou, 2019; Li and Zhou, 2020; Bartyik et al., 2021). Nevertheless, several studies demonstrated controversial phenomena in which QLS does not increase with the number of IBCs (Fitzsimmons, 2011; Sawakuchi et al., 2018). There is insufficient evidence to suggest that differences in IBC can be explained by differences between weathering alone. However, the QLS of the eight samples tended to increase gradually with the number of IBCs, while maintaining a good consistency. This indicates that although the quartz has undergone different grades of *in-situ* chemical weathering, it maintains a consistent response to IBC, which may facilitate the subsequent use of IBC for source tracing or geomorphic process analysis.

The heating rate and the time held at high temperatures together affect the shape and peak position of the TAC (Aitken, 1985). To facilitate comparison, all the TAC data of the current study were obtained by the same thermal treatment. Aitken (1985) assumed that the TAC reflects the distribution of reservoir traps (R) and luminescence traps (L), both of which were proposed by Zimmerman (1971). He also suggested that R traps close to the valence band have their holes transferred to the L centers at a lower temperature than traps that are not as close. Many studies have taken advantage of this feature and concluded that TAC can distinguish the source of sediments (Zheng et al., 2009; Chang and Zhou, 2019; Nian et al., 2019; Li and Zhou, 2020). In contrast, our study shows that the TAC of quartz differs significantly even from that of the same rock mass, especially in the Sanming borehole (Figure 3 and Section 4.3). Considering the large differences between *in situ* weathering residuals and sediments, we are unable to

conclude the TAC characteristics of quartz from the same rock mass after geomorphic processes such as denudation and transport.

6 CONCLUSION

In this study, eight samples from areas of intense chemical weathering were used to analyze the constraints of chemical weathering processes on QLS. The quartz 110°C TL sensitivity is more sensitive to chemical weathering relative to OSL sensitivity, although this tendency to enhance with chemical weathering is limited in our drilled samples. The samples from the upper part of the borehole that experienced stronger chemical weathering had more fast component than the samples from the bottom, but not significantly. Using the weathering rates of similar areas, we assumed that the QLS does not receive obvious alterations from *in situ* chemical weathering within 200 ka. We have found that quartz from the same source undergoes different degrees of *in situ* chemical weathering, but maintains a consistent response to IBC, which may also be a beneficial tool for geomorphic analysis. The thermal activation curve (TAC) results of the same rock mass show large differences, shaking the reliability of TAC as a provenance indicator. However, considering the differences between sediments and *in situ* weathering residuals, the reliability of TAC as a provenance indicator needs further study.

REFERENCES

- Adamic, G., and Aitken, M. J. (1998). Dose-Rate Conversion Factors: Update. *Anc. TL* 16 (2), 37–50.
- Aitken, M. J. (1998). *An Introduction to Optical Dating: The Dating of Quaternary Sediments by the Use of Photon-Stimulated Luminescence*. Oxford: Oxford University Press.
- Aitken, M. J. (1985). *Thermoluminescence Dating*. London: Academic Press.
- Armitage, S. J., Duller, G. A. T., and Wintle, A. G. (2000). Quartz from Southern Africa: Sensitivity Changes as a Result of Thermal Pretreatment. *Radiat. Meas.* 32 (5–6), 571–577. doi:10.1016/S1350-4487(00)00053-6
- Bartyik, T., Magyar, G., Filyó, D., Tóth, O., Blanka-Végi, V., Kiss, T., et al. (2021). Spatial Differences in the Luminescence Sensitivity of Quartz Extracted from Carpathian Basin Fluvial Sediments. *Quat. Geochronol.* 64, 101166. doi:10.1016/j.quageo.2021.101166
- Benny, P. G., Sanjeev, N., Gundu Rao, T. K., and Bhatt, B. C. (2000). Gamma Ray Induced Sensitization of 110°C TL Peak in Quartz Separated from Sand. *Radiat. Meas.* 32 (3), 247–252. doi:10.1016/S1350-4487(99)00268-1
- Bluszcz, A., and Adamic, G. (2006). Application of Differential Evolution to Fitting OSL Decay Curves. *Radiat. Meas.* 41 (7), 886–891. doi:10.1016/j.radmeas.2006.05.016
- Botter-Jensen, L., Agersnap Larsen, N., Mejdahl, V., Poolton, N. R. J., Morris, M. F., and McKeever, S. W. S. (1995). Luminescence Sensitivity Changes in Quartz as a Result of Annealing. *Radiat. Meas.* 24 (4), 535–541. doi:10.1016/1350-4487(95)00006-z
- Bureau of Geology and Mineral Resources of Fujian Province (1985). *Regional Geology of Fujian Province*. Beijing: Geological Publishing House.
- Chang, Z., and Zhou, L. (2019). Evidence for Provenance Change in Deep Sea Sediments of the Bengal Fan: A 7 Million Year Record from IODP U1444A. *J. Asian Earth Sci.* 186, 104008. doi:10.1016/j.jseas.2019.104008

DATA AVAILABILITY STATEMENT

The original contributions presented in the study are included in the article/**Supplementary Material**, further inquiries can be directed to the corresponding author.

AUTHOR CONTRIBUTIONS

ZC contributed to conception and design of the study. ZC, YJ, and JX performed the statistical analysis. JZ organized the fieldwork. ZC, JX, and CZ organized the experiment. ZC wrote the first draft of the manuscript. All authors contributed to manuscript revision, read, and approved the submitted version.

ACKNOWLEDGMENTS

We are grateful to Professor Liping Zhou for his valuable comments and helpful discussions during this work. We also thank the two reviewers, whose constructive comments made the manuscript a great improvement.

SUPPLEMENTARY MATERIAL

The Supplementary Material for this article can be found online at: <https://www.frontiersin.org/articles/10.3389/feart.2022.940212/full#supplementary-material>

- Chauhan, N., and Singhvi, A. K. (2019). Changes in the Optically Stimulated Luminescence (OSL) Sensitivity of Single Grains of Quartz During the Measurement of Natural OSL: Implications for the Reliability of Optical Ages. *Quat. Geochronol.* 53, 101004. doi:10.1016/j.quageo.2019.101004
- del Río, I., Sawakuchi, A. O., Góes, A. M., Hollanda, M. H. B. M., Furukawa, L. Y., Porat, N., et al. (2021). Luminescence Signals of Quartz and Feldspar as New Methods for Stratigraphic Discrimination and Provenance Analysis of Siliciclastic Successions: The Case of the Parnaíba Basin (Brazil) of West Gondwana. *Basin Res.* 33 (6), 2938–2959. doi:10.1111/bre.12590
- Duller, G. A. T. (2003). Distinguishing Quartz and Feldspar in Single Grain Luminescence Measurements. *Radiat. Meas.* 37 (2), 161–165. doi:10.1016/S1350-4487(02)00170-1
- Fitzsimmons, K. (2011). An Assessment of the Luminescence Sensitivity of Australian Quartz with Respect to Sediment History. *Geochronometria* 38 (3), 199–208. doi:10.2478/s13386-011-0030-9
- Fuchs, M., and Owen, L. A. (2008). Luminescence Dating of Glacial and Associated Sediments: Review, Recommendations and Future Directions. *Boreas* 37 (4), 636–659. doi:10.1111/j.1502-3885.2008.00052.x
- Guérin, G., Mercier, N., and Adamic, G. (2011). Dose-Rate Conversion Factors: Update. *Anc. TL* 29 (1), 5–8.
- Gupta, A. S., and Rao, S. K. (2001). Weathering Indices and Their Applicability for Crystalline Rocks. *Bull. Eng. Geol. Environ.* 60 (3), 201–221. doi:10.1007/s100640100113
- Higashimura, T., Ichikawa, Y., and Sidei, T. (1963). Dosimetry of Atomic Bomb Radiation in Hiroshima by Thermoluminescence of Roof Tiles. *Science* 139 (3561), 1284–1285. doi:10.1126/science.139.3561.1284.b
- Ike, P. O., Folley, D. E., Agwu, K. K., Chithambo, M. L., Chikwembani, S., and Ezema, F. I. (2021). Influence of Dysprosium Doping on the Structural, Thermoluminescence and Optical Properties of Lithium Aluminium Borate. *J. Lumin.* 233, 117932. doi:10.1016/j.jlumin.2021.117932

- Jeong, G. Y., Cheong, C.-S., and Choi, J.-H. (2007). The Effect of Weathering on Optically Stimulated Luminescence Dating. *Quat. Geochronol.* 2 (1-4), 117–122. doi:10.1016/j.quageo.2006.05.023
- Kalita, J. M., Thomas, S., and Chithambo, M. L. (2019). Thermally and Optically Stimulated Luminescence of Natural Red and Blue Corundum (Al₂O₃). *J. Luminescence* 205, 417–422. doi:10.1016/j.jlumin.2018.09.058
- Kortekaas, M., and Murray, A. S. (2005). A Method for the Removal of Mica from Quartz Separates. *Anc. TL* 23 (2), 43–46.
- Lai, Z. (2006). Testing the Use of an OSL Standardised Growth Curve (SGC) for Determination on Quartz from the Chinese Loess Plateau. *Radiat. Meas.* 41 (1), 9–16. doi:10.1016/j.radmeas.2005.06.031
- Li, J., Zhang, Y., Dong, S., and Johnston, S. T. (2014). Cretaceous Tectonic Evolution of South China: A Preliminary Synthesis. *Earth-Science Rev.* 134, 98–136. doi:10.1016/j.earscirev.2014.03.008
- Li, S.-H., Chen, Y.-Y., Li, B., Sun, J., and Yang, L.-R. (2007). OSL Dating of Sediments from Deserts in Northern China. *Quat. Geochronol.* 2 (1-4), 23–28. doi:10.1016/j.quageo.2006.05.034
- Li, S.-H., and Wintle, A. G. (1992). Luminescence Sensitivity Change Due to Bleaching of Sediments. *Int. J. Radiat. Appl. Instrum. Part D. Nucl. Tracks Radiat. Meas.* 20 (4), 567–573. doi:10.1016/1359-0189(92)90006-h
- Li, Y., and Zhou, L. (2020). Variations of Thermally and Optically Stimulated Luminescence Sensitivity of Loess and Pedocomplex Samples from Southern Tajikistan, Central Asia. *Geochronometria* 48 (1), 242–252. doi:10.1515/geochr-2015-0118
- Li, Z.-X., Li, X.-h., Zhou, H., and Kinny, P. D. (2002). Grenvillian Continental Collision in South China: New SHRIMP U-Pb Zircon Results and Implications for the Configuration of Rodinia. *Geology* 30 (2), 163–166. doi:10.1130/0091-7613(2002)030<0163:ggcisc>2.0.co;2
- Lü, T., Sun, J., Feathers, J. K., and Sun, D. (2020). Spatiotemporal Variations and Implications of Luminescence Sensitivity of Quartz Grains on the Chinese Loess Plateau since the Last Interglaciation. *Quat. Res.* 99, 190–203. doi:10.1017/qua.2020.53
- Lü, T., Sun, J., Li, S.-H., Gong, Z., and Xue, L. (2014). Vertical Variations of Luminescence Sensitivity of Quartz Grains from Loess/Paleosol of Luochuan Section in the Central Chinese Loess Plateau Since the Last Interglacial. *Quat. Geochronol.* 22, 107–115. doi:10.1016/j.quageo.2014.04.004
- Lü, T., and Sun, J. (2017). Luminescence Sensitivities of Quartz Grains from Eolian Deposits in Northern China and Their Implications for Provenance. *Quat. Res.* 76 (2), 181–189. doi:10.1016/j.yqres.2011.06.015
- Murray, A. S., and Wintle, A. G. (2000). Luminescence Dating of Quartz Using an Improved Single-Aliquot Regenerative-Dose Protocol. *Radiat. Meas.* 32 (1), 57–73. doi:10.1016/S1350-4487(99)00253-X
- Murray, A. S., and Wintle, A. G. (2003). The Single Aliquot Regenerative Dose Protocol: Potential for Improvements in Reliability. *Radiat. Meas.* 37 (4-5), 377–381. doi:10.1016/S1350-4487(03)00053-2
- Nelson, M. S., Eppes, M. C., and Rittenour, T. M. (2022). Quartz Luminescence Sensitivity from Sediment versus Bedrock in Highly Weathered Soils of the Piedmont of North Carolina, South-Eastern USA. *Quat. Geochronol.* 72, 101343. doi:10.1016/j.quageo.2022.101343
- Nesbitt, H. W. (1979). Mobility and Fractionation of Rare Earth Elements During Weathering of a Granodiorite. *Nature* 279 (5710), 206–210. doi:10.1038/279206a0
- Nesbitt, H. W., and Young, G. M. (1982). Early Proterozoic Climates and Plate Motions Inferred from Major Element Chemistry of Lutites. *Nature* 299 (5885), 715–717. doi:10.1038/299715a0
- Nian, X., Zhang, W., Qiu, F., Qin, J., Wang, Z., Sun, Q., et al. (2019). Luminescence Characteristics of Quartz from Holocene Delta Deposits of the Yangtze River and Their Provenance Implications. *Quat. Geochronol.* 49, 131–137. doi:10.1016/j.quageo.2018.04.010
- Parker, A. (1970). An Index of Weathering for Silicate Rocks. *Geol. Mag.* 107 (6), 501–504. doi:10.1017/s0016756800058581
- Peng, J., Dong, Z., Han, F., Long, H., and Liu, X. (2013). R Package numOSL: Numeric Routines for Optically Stimulated Luminescence Dating. *Anc. TL* 31 (2), 41–48.
- Pietsch, T. J., Olley, J. M., and Nanson, G. C. (2008). Fluvial Transport as a Natural Luminescence Sensitiser of Quartz. *Quat. Geochronol.* 3 (4), 365–376. doi:10.1016/j.quageo.2007.12.005
- Pires, E. L., Tatum, S. H., Mittani, J. C. R., Kinoshita, A., Baffa, O., and Caldas, L. V. E. (2011). TL, OSL and ESR Properties of Nanostructured KAlSi₃O₈:Mn Glass. *Radiat. Meas.* 46, 1492–1495. doi:10.1016/j.radmeas.2011.04.041
- Preusser, F., Ramseyer, K., and Schlüchter, C. (2006). Characterisation of Low OSL Intensity Quartz from the New Zealand Alps. *Radiat. Meas.* 41 (7-8), 871–877. doi:10.1016/j.radmeas.2006.04.019
- Qiu, F., and Zhou, L. (2015). A New Luminescence Chronology for the Mangshan Loess-Paleosol Sequence on the Southern Bank of the Yellow River in Henan, Central China. *Quat. Geochronol.* 30, 24–33. doi:10.1016/j.quageo.2015.06.014
- Reiche, P. (1943). Graphic Representation of Chemical Weathering. *J. Sediment. Res.* 13 (2), 58–68. doi:10.1306/d4269198-2b26-11d7-8648000102c1865d
- Rendell, H. M., Townsend, P. D., Wood, R. A., and Luff, B. J. (1994). Thermal Treatments and Emission-Spectra of TL from Quartz. *Radiat. Meas.* 23 (2-3), 441–449. doi:10.1016/1350-4487(94)90077-9
- Richter, D., Pintaske, R., Dornich, K., and Krbetschek, M. (2012). A Novel Beta Source Design for Uniform Irradiation in Dosimetric Applications. *Anc. TL* 30 (2), 57–63.
- Richter, D., Richter, A., and Dornich, K. (2013). Lexsyg - A New System for Luminescence Research. *Geochronometria* 40 (4), 220–228. doi:10.2478/s13386-013-0110-0
- Rink, W. J. (1994). Billion-Year Age-Dependence of Luminescence in Granitic Quartz. *Radiat. Meas.* 23 (2-3), 419–422. doi:10.1016/1350-4487(94)90074-4
- Ruxton, B. P. (1968). Measures of the Degree of Chemical Weathering of Rocks. *J. Geol.* 76 (5), 518–527. doi:10.1086/627357
- Sawakuchi, A. O., Blair, M. W., DeWitt, R., Faleiros, F. M., Hyppolito, T., and Guedes, C. C. F. (2011a). Thermal History versus Sedimentary History: OSL Sensitivity of Quartz Grains Extracted from Rocks and Sediments. *Quat. Geochronol.* 6 (2), 261–272. doi:10.1016/j.quageo.2010.11.002
- Sawakuchi, A. O., DeWitt, R., and Faleiros, F. M. (2011b). Correlation Between Thermoluminescence Sensitivity and Crystallization Temperatures of Quartz: Potential Application in Geothermometry. *Radiat. Meas.* 46 (1), 51–58. doi:10.1016/j.radmeas.2010.08.005
- Sawakuchi, A. O., Jain, M., Mineli, T. D., Nogueira, L., Bertassoli, D. J., Häggi, C., et al. (2018). Luminescence of Quartz and Feldspar Fingerprints Provenance and Correlates with the Source Area Denudation in the Amazon River Basin. *Earth Planet. Sci. Lett.* 492, 152–162. doi:10.1016/j.epsl.2018.04.006
- Sawakuchi, A. O., Rodrigues, F. C. G., Mineli, T. D., Mendes, V. R., Melo, D. B., Chiessi, C. M., et al. (2020). Optically Stimulated Luminescence Sensitivity of Quartz for Provenance Analysis. *Methods Protoc.* 3 (1), 6. doi:10.3390/mps3010006
- Schulz, M. S., and White, A. F. (1999). Chemical Weathering in a Tropical Watershed, Luquillo Mountains, Puerto Rico III: Quartz Dissolution Rates. *Geochim. Cosmochim. Acta* 63 (3-4), 337–350. doi:10.1016/S0016-7037(99)00056-3
- Shu, L. (2012). An Analysis of Principal Features of Tectonic Evolution in South China Block. *Geol. Bull. China* 31 (7), 1035–1053. (Chinese with English Abstract).
- Shu, L. (2006). Predevonian Tectonic Evolution of South China: From Cathaysian Block to Caledonian Period Folded Orogenic Belt. *Geol. J. China Univ.* 12 (4), 418–431. (Chinese with English Abstract).
- Shu, L., Yao, J., Wang, B., Faure, M., Charvet, J., and Chen, Y. (2021). Neoproterozoic Plate Tectonic Process and Phanerozoic Geodynamic Evolution of the South China Block. *Earth-Sci. Rev.* 216, 103596. doi:10.1016/j.earscirev.2021.103596
- Singhvi, A. K., Sharma, Y. P., and Agrawal, D. P. (1982). Thermoluminescence Dating of Sand Dunes in Rajasthan, India. *Nature* 295 (5847), 313–315. doi:10.1038/295313a0
- Smith, B. W., and Rhodes, E. J. (1994). Charge Movements in Quartz and Their Relevance to Optical Dating. *Radiat. Meas.* 23 (2-3), 329–333. doi:10.1016/1350-4487(94)90060-4
- Sueoka, T., Lee, I., Muramatsu, M., and Imamura, S. (1985). “Geomechanical Properties and Engineering Classification for Decomposed Granite Soils in Kaduna District, Nigeria,” in Proceedings of the First International Conference on Geomechanics in Tropical Lateritic and Saprolitic Soils, Brasilia, February 11–14, 1985, 175–186.
- Takaku, J., Tadono, T., Doutsu, M., Ohgushi, F., and Kai, H. (2020). Updates of ‘Aw3D30’ Alos Global Digital Surface Model with Other Open Access Datasets. *Int. Arch. Photogramm. Remote Sens. Spat. Inf. Sci.* XLIII-B4-2020, 183–189. doi:10.5194/isprs-archives-XLIII-B4-2020-183-2020

- Vaitkus, A., Merkys, A., and Gražulis, S. (2021). Validation of the Crystallography Open Database Using the Crystallographic Information Framework. *J. Appl. Cryst.* 54 (2), 661–672. doi:10.1107/s1600576720016532
- Warr, L. N. (2021). IMA-CNMNC Approved Mineral Symbols. *Mineral. Mag.* 85 (3), 291–320. doi:10.1180/mgm.2021.43
- Yang, H., and Zhou, S. (2019). Application of Uranium Disequilibrium in the Study of the Weathering Rate of the Granite in Northern Guangdong. *J. South China Normal Univ. Nat. Sci. Ed.* 51 (5), 84–91. (Chinese with English Abstract). doi:10.6054/j.jscn.2019088
- Yukihara, E. G., and McKeever, S. W. S. (2008). Optically Stimulated Luminescence (OSL) Dosimetry in Medicine. *Phys. Med. Biol.* 53 (20), R351–R379. doi:10.1088/0031-9155/53/20/r01
- Zhang, Y., Xu, X., Jia, D., and Shu, L. (2009). Deformation Record of the Change from Indosinian Collision-Related Tectonic System to Yanshanian Subduction-Related Tectonic System in South China During the Early Mesozoic. *Earth Sci. Front.* 16 (1), 234–247. (Chinese with English Abstract).
- Zheng, C., Zhou, L., and Qin, J. (2009). Difference in Luminescence Sensitivity of Coarse-Grained Quartz from Deserts of Northern China. *Radiat. Meas.* 44 (5-6), 534–537. doi:10.1016/j.radmeas.2009.02.013
- Zhou, L., Fu, D., and Zhang, J. (2010). An Analysis of the Components of the Luminescence Signals of Selected Polymineral and Quartz Samples from Loess in Western China and Southern Tajikistan, and Their Suitability for Optical Dating. *Quat. Geochronol.* 5 (2-3), 149–153. doi:10.1016/j.quageo.2009.05.008
- Zhou, L., and Wintle, A. G. (1994). Sensitivity Change of Thermoluminescence Signals After Laboratory Optical Bleaching - Experiments with Loess Fine Grains. *Quat. Sci. Rev.* 13 (5-7), 457–463. doi:10.1016/0277-3791(94)90058-2
- Zimmerman, J. (1971). The Radiation-Induced Increase of the 100°C Thermoluminescence Sensitivity of Fired Quartz. *J. Phys. C. Solid State Phys.* 4 (18), 3265–3276. doi:10.1088/0022-3719/4/18/032
- Zu, F., Shu, L., and Li, C. (2012). Evolution Features of Depositional and Tectonic Setting from Late Paleozoic to Meso—Cenozoic in the Yong'an Basin. *Geol. Rev.* 58 (01), 126–148. (Chinese with English Abstract). doi:10.16509/j.georeview.2012.01.005

Conflict of Interest: The authors declare that the research was conducted in the absence of any commercial or financial relationships that could be construed as a potential conflict of interest.

Publisher's Note: All claims expressed in this article are solely those of the authors and do not necessarily represent those of their affiliated organizations, or those of the publisher, the editors and the reviewers. Any product that may be evaluated in this article, or claim that may be made by its manufacturer, is not guaranteed or endorsed by the publisher.

Copyright © 2022 Cao, Jiang, Xu, Zhao and Zhao. This is an open-access article distributed under the terms of the Creative Commons Attribution License (CC BY). The use, distribution or reproduction in other forums is permitted, provided the original author(s) and the copyright owner(s) are credited and that the original publication in this journal is cited, in accordance with accepted academic practice. No use, distribution or reproduction is permitted which does not comply with these terms.